BLAST WAVE TIME OF ARRIVAL:
A RELIABLE METRIC TO DETERMINE PRESSURE AND YIELD OF HIGH EXPLOSIVE DETONATIONS

Written by:
S. E. Rigby
University of Sheffield, Department of Civil & Structural Engineering, UK

Abstract

The provision of robust and resilient blast protective systems requires detailed knowledge of the form and magnitude of blast loading that the structure is expected to protect against. Blast wave time of arrival is not typically required when assessing structural response to explosive loading and therefore is often overlooked in favour of other parameters such as peak pressure and impulse. However, well-known velocity-dependent relationships can be used to infer many different blast characteristics from arrival time measurements, offering key insights into the behaviour of a blast wave as it propagates. Furthermore, time of arrival can be quantified with higher precision and higher fidelity when compared to other loading parameters, as is shown in this article. Recent advancements in experimental techniques such as high speed video enable high-rate, full-field measurement of blast wave arrival time.

This article reports a number of arrival time studies conducted by the author and colleagues. In particular, arena testing is used to make comments on the reliability of time of arrival measurements, and two recent examples are provided. In the first, arrival time measurements are used to infer near-field reflected blast pressure distributions, and in the second arrival time measurements are used to estimate the yield of the 2020 Beirut explosion. This article aims to demonstrate the versatility, accuracy, and importance of arrival time measurements, and the insights that such information can offer.

Keywords: Beirut explosion; Blast; Experimentation; Time of arrival

Introduction

Accurate quantification of the form and magnitude of loading imparted to a structure following detonation of a high explosive is a crucial first step in protection engineering design. Experimental measurement of blast wave parameters has been an active area of research since the mid-1940s [1], with a large number of these early studies compiled into the now industry-standard Kingery and Bulmash formulae [2] and the ConWep predictive tool [3]. These well-established methodologies enable blast pressure loads to be generated for a wide range of scenarios; from near-contact to far-field, and for free-air or surface bursts.

Whilst peak pressure/force, loading duration, and specific/total impulse are all important parameters when assessing structural response, blast wave time of arrival (TOA) is a reliable metric[1] which can provide key insights into the behaviour of a blast wave. Since pressure and velocity are interdependent, if the velocity of a blast wave is known (or determined from TOA measurements at different locations), its pressure can be inferred. Knowledge of the pressure-velocity relationship of an air shock, typically derived from a series of Rankine-Hugoniot jump conditions [4], has enabled researchers to determine near-field blast pressures [5, 6], and, more recently, to study blast behaviour in greater detail using optical methods [7-11].

This article summarises recent research by the author on the topic of blast wave time of arrival. Firstly, high repeatability of TOA measurements is demonstrated through a compilation of far-field

---

[1]Often, interpretation of the peak pressure and duration of a recorded signal is made difficult by sensor ringing and electrical noise. The arrival time of a blast wave, however, is typically recorded as a sharp, unambiguous, and relatively instantaneous rise above ambient conditions, making precise determination of TOA possible.

arena testing. Subsequently, two studies are discussed, where TOA was used to infer near-field reflected blast pressure distributions, and to estimate the yield of the 2020 Beirut explosion.

Far-field experimental studies

In recent years, the author and colleagues at the University of Sheffield (UoS) Blast and Impact Laboratory have conducted approximately 80 far-field arena tests using hemispheres of PE4 explosive, a number of which have previously been published [12-16]. A photograph from a typical far-field arena test is shown in Figure 1. The charges were formed using bespoke 3D printed charge moulds, and were placed on a small (approximately 200 × 200 × 50 mm) steel anvil prior to detonation to avoid repeat damage to the concrete ground slab. The charges were located between 1.25-10.00 m from the blockwork-covered external wall of a reinforced concrete bunker, and were positioned using a laser range meter to ensure accurate charge placement.

Pressure histories were recorded using Kulite HKM-375 piezoresistive pressure gauges flush with the surface of small steel plates affixed to the blockwork wall. A number of different pressure gauge placements have been used:

- ↘ A pair of pressure gauges located at ground level, with each gauge slightly off-centre (< 50 mm) from the line intersecting the charge centre;
- ↘ A single pressure gauge located at ground level, directly in line with the charge centre;
- ↘ As above, with the addition of two ground-level gauges at 2 m and 3 m lateral distance respectively from the central gauge, and a single gauge placed 2 m directly above the central gauge (the arrangement shown in Figure 1). Here, the assumption is that the shock waves are sufficiently weak such that the time of arrival to an oblique gauge is dictated by the incident conditions

along the hypotenuse distance to the charge centre, and is unaffected by reflection of the blast wave at shallower angles of incidence.

Pressure was recorded using a 16-bit digital oscilloscope at a typical sample rate of 200 kHz and 14-bit resolution. Recording was triggered via a voltage drop in a breakwire wrapped around the detonator to synchronise recordings with initiation of the charge. In total, 157 TOA measurements were recorded from tests using 180-350 g PE4 hemispheres and have been compiled in this study. Results are expressed at 1 kg scale in Figure 2(a) using Hopkinson-Cranz scaling [17, 18] and compared to ConWep predictions for 1.2 kg TNT assuming an equivalence of 1.20 for PE4 [19, 20], giving a range of scaled distances between 1.9-14.9 $m/kg^{1/3}$. It can be seen that the ConWep curve is a close match for the experimental values across the entire range of scaled distances studied.

Also shown in Figure 2(b) are the residuals, i.e. the difference between observed (experimental) and predicted (ConWep) TOAs. At the median scaled distance, 5.5 $m/kg^{1/3}$, the maximum residual of ±0.2 $ms/kg^{1/3}$ corresponds to a relative difference in TOA of approximately ±2%. This is considerably lower than typical variations of 6-8% seen in peak pressure and peak specific impulse data [12], and confirms that TOA measurements are more repeatable and better predicted by ConWep compared to other blast parameters, by some margin.

Near-field experimental studies and analytical work

Determining time of arrival using image processing

Near-field tests at the UoS Blast and Impact Laboratory have focussed on quantifying the loading distributions from high explosives located close to a nominally rigid reflecting surface. The *Characterisation*
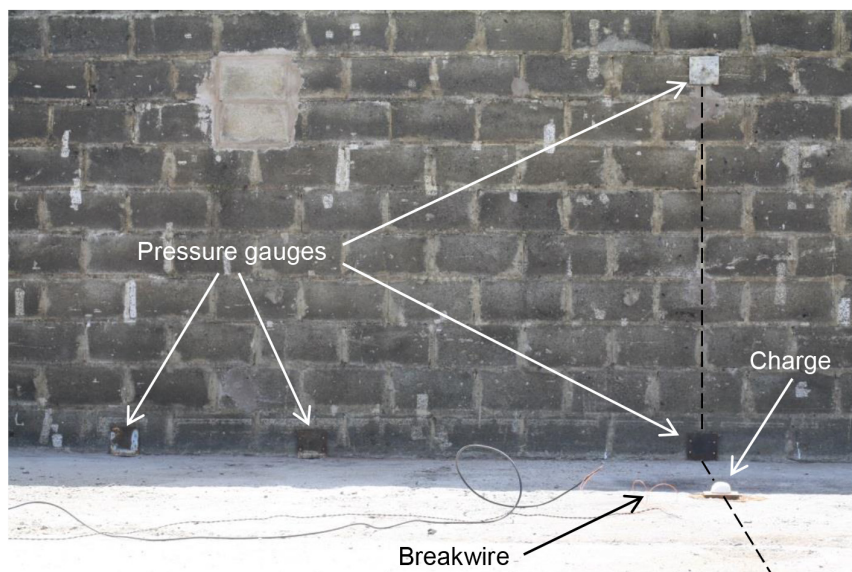

Figure 1   Far-field arena test set up [12]

of Blast Loading (CoBL) apparatus [21] was initially designed to measure the loading output from shallow buried explosives [22], but has also been used to study free-air explosions [23] and explosions in reduced pressure or reduced oxygen environments [24].

The CoBL apparatus, shown in Figure 3(a) comprises a pair of steel fibre and bar reinforced concrete frames, set approximately 1 m apart, with a 1400 mm diameter, 100 mm thick mild steel target spanning between the undersides of each frame. The plate is drilled through its thickness, with the 10.5 mm holes forming a '+' arrangement when viewed on plan, see Figure 3(b). The holes are spaced at 25 mm (centre-to-centre) along the four arrays which extend out from the common central hole. 3.25 m long, 10 mm diameter Hopkinson pressure bars (HPBs) are suspended from their distal ends such that their faces lie flush with the underside of the target plate, which acts as a nominally rigid reflecting surface during the tests. Typically, 17 HPBs are located within the 200 mm diameter

instrumented region: one central bar and four bars each at 25 mm, 50 mm, 75 mm, and 100 mm from the plate centre.

In addition to direct load measurements from the HPBs, a Photron FASTCAM SA-Z high speed video camera (HSV) enables evolution of the detonation product fireball and interaction with the target surface to be filmed. In a recent study [25], 100 g PE4 charges were formed into spheres (again using bespoke 3D printed charge moulds) and suspended on a glass-fibre weave fabric 'drumskin' (25 g/m² area density), held taught in a steel ring at 380 mm normal distance from the underside of the target plate. Three tests were performed in total, recorded at 160,000 fps with 280×256 pixel resolution. The camera was positioned approximately level in height with the centre of the charge, with the vertical field-of-view set between the charge centre and the underside of the target plate. As with the far-field tests, recording was synchronised with detonation by triggering off a breakwire wrapped around the detonator.
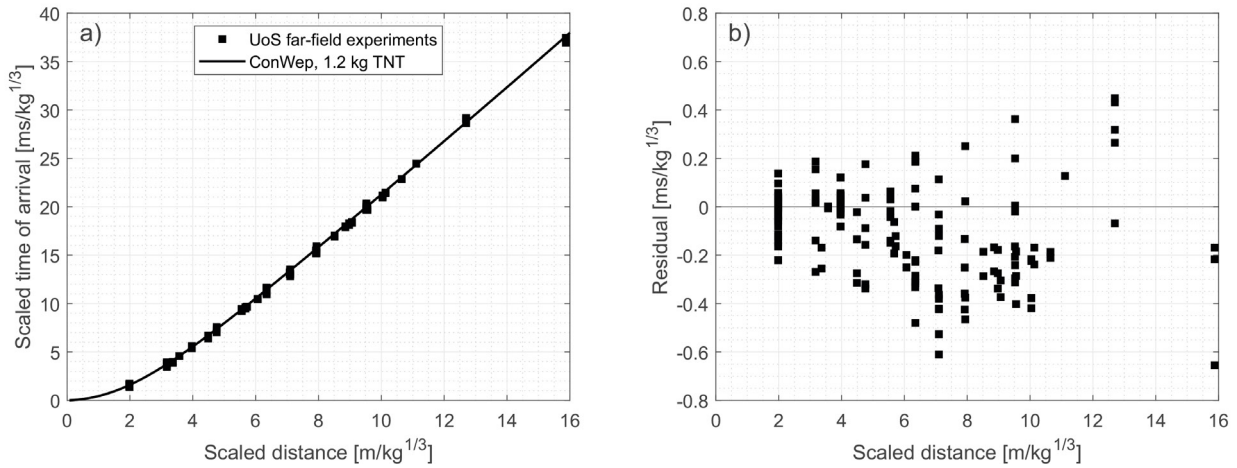

Figure 2   a) Blast wave time of arrival from UoS far-field arena tests using 180-350 g hemispheres of PE4 [12-16], expressed at 1 kg scale and compared to ConWep predictions for 1.2 kg TNT hemisphere assuming an equivalence of 1.20; b) Residual: difference between observed and predicted data shown in (a)
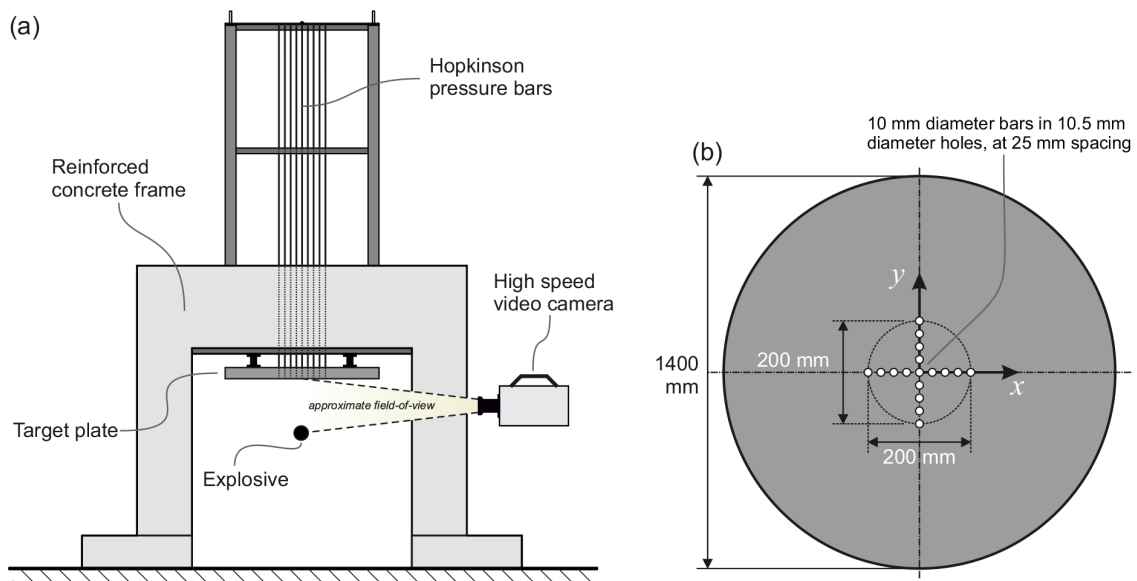

Figure 3   Schematic of Characterisation of Blast Loading apparatus [21]: (a) elevation; (b) detailed plan view of target plate showing bar arrangement. Figure adapted from Ref. [25]. Note: camera positioning is indicative.
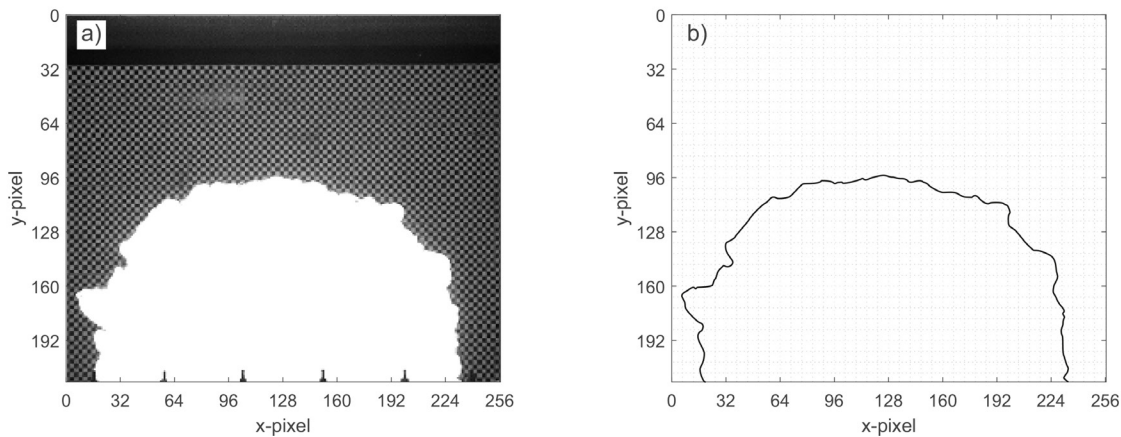
Figure 4   a) Example frame from high speed video footage; b) Resulting fireball edge detection using the Canny algorithm. Figure adapted from Ref. [25]

The tests were self-illuminated by the incandescence of the detonation product cloud, and a clear distinction between the fireball and surrounding air was visible. From these images, processing techniques such as the Canny edge detection algorithm [26] can be used to determine the location of the fireball edge in each frame. An example of this is shown in Figure 4.

The fireball radius was evaluated along a series of 'spokes' emanating from the charge centre at regular angles. This allowed the average fireball radius to be determined as a function of time, with the mean radius-time relationship from the three tests shown in Figure 5. This relationship is compared to ConWep predictions for a 0.12 kg TNT sphere, again assuming an equivalence of 1.20 for PE4 [19, 20]. Despite being highly accurate in the far-field, near-field ConWep TOA predictions are not in good agreement with the experimental data. It is clear that more work is required to determine precise TOA relationships for different explosives in the extreme near-field.
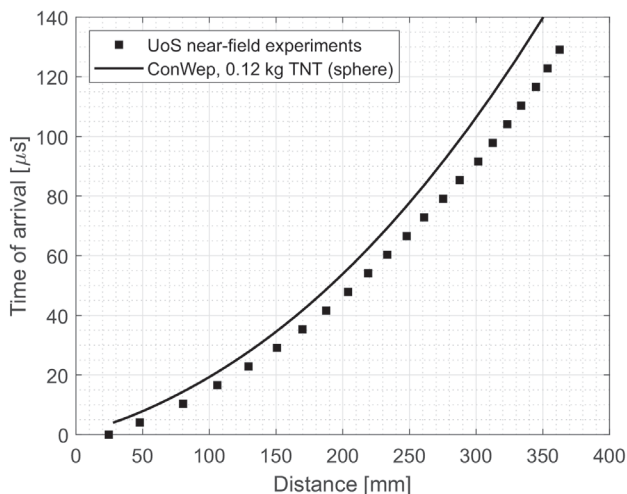

Figure 5   Mean fireball radius vs. time relationship determined from near-field image tracking experiments [25] compared to ConWep predictions for 0.12 kg TNT (sphere) assuming an equivalence of 1.20

Calculating reflected pressure distributions using time of arrival

The incident radius-time relationship shown in Figure 5 can be used to calculate *reflected* pressure distributions, as in Rigby *et al*. [25], through manipulation of the Rankine-Hugoniot jump conditions available in many sources, e.g. [4].

The peak overpressure[2] of an incident blast wave, p_i, can be expressed as a function of ambient pressure, p_a, and Mach number[3], M_i [4]:

$$p_i = p_a \frac{7(M_i^2 - 1)}{6} \tag{1}$$

Peak *oblique* reflected overpressure, $p_{r,\theta}$, i.e. the peak pressure acting at any point of non-normal impingement on a target surface, is dependent on incident Mach number and angle of incidence, θ, defined as the angle between the outward normal of the surface and the direct vector from the explosive charge to that point [14]:

$$p_{r,\theta} = p_a \left[\frac{(7M_{r,\theta}^2 - 1)(7M_i^2 - 1)}{36} - 1 \right] \tag{2}$$

Where p_a and M_i are as before, and $M_{r,\theta}$ is the oblique reflected Mach number. In order to calculate the oblique reflected Mach number, the problem is represented as a steady-flow counterpart, as in Figure 6.
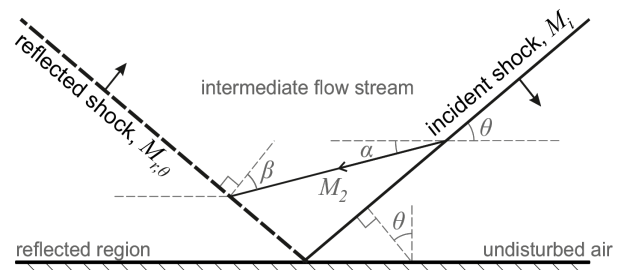

Figure 6   Steady-flow counterpart of oblique shock reflection. Figure adapted from Ref. [25]

---

[2]Peak pressure minus ambient pressure.
[3]Shock velocity divided by sonic velocity.

Here, α is the stream deflection angle, β, is the angle that the intermediate stream enters the reflected region, and M_2 is the stream Mach number, which is related to the oblique Mach number through the following expression:

$$M_{r,\theta} = M_2 \sin\theta \qquad (3)$$

First, α can be calculated as a function of angle of incidence and incident Mach number:

$$\frac{\tan(\theta - \alpha)}{\tan\theta} = \frac{M_i^2 + 5}{6M_i^2} \qquad (4)$$

This allows the stream Mach number, M_2, to be calculated:

$$M_2 \sin(\theta - \alpha) = \sqrt{\frac{M_i^2 + 5}{7M_i^2 - 1}} \qquad (5)$$

And finally, the stream deflection angle, β, can be calculated through iteration of the following expression:

$$\frac{\tan(\beta - \alpha)}{\tan\beta} = \frac{5 + (M_2 \sin\beta)^2}{6(M_2 \sin\beta)^2} \qquad (6)$$

The above methodology can be used to infer peak pressure distributions by evaluating Equation (2) at a number of points on the reflecting surface. As a verification exercise, the radius-time relationship derived in this work for 100 g PE4 spheres[4], as in Figure 5, was used to evaluate incident Mach numbers[5] impinging on the surface of a rigid target located 80 mm normal distance from the centre of the explosive; a repeat of the experiments reported in Rigby *et al.* [27] where peak oblique pressures were directly measured using the CoBL apparatus.

The results of this exercise are shown in Figure 7, where 'HPB' denotes the directly-measured pressures using Hopkinson pressure bars [27], and 'HSV' denotes the high-speed video inferred pressures according to the methodology described above.

Generally the HSV pressure distributions closely follow those from the HPB measurements, with the magnitude and shape of the pressure distribution curve being well predicted. A statistical analysis showed that 50 of the 51 HPB peak pressures (three tests using 17 HPBs in each) were within two standard deviations of the HSV peak pressures,
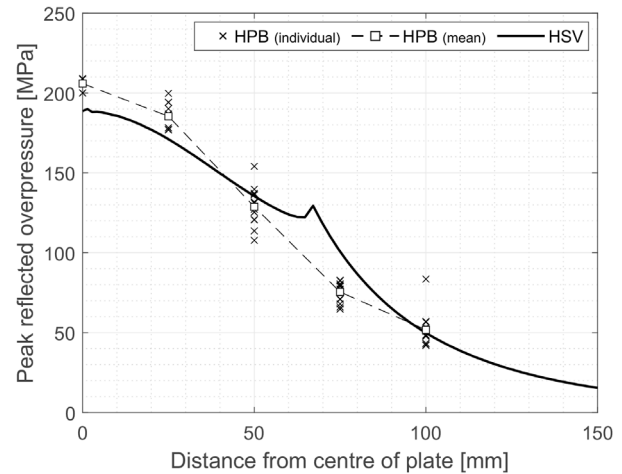

Figure 7   Inferred reflected pressure distribution along a flat, rigid target located at 80 mm normal distance from the explosive centre (HSV), compared to directly-measured reflected pressures (HPB). Figure adapted from Ref. [25]

and the mean HPB pressures were within 10% of the HSV values for all recording locations except for at 75 mm from the plate centre.

These results are highly significant as they demonstrate that using the method summarised in this article (and first outlined in Ref. [25]) can yield accurate predictions of reflected pressure distributions along a target surface, using only video footage of free-air fireball expansion. Essentially, this method is truly non-intrusive, and surface pressure can be 'measured' on any hypothetical target from only a single test (or a small number of repeats), provided that TOA can be accurately quantified at a range of distances from the charge centre.

Estimating the yield of the 2020 Beirut explosion using social media video footage

On the 4th August 2020 a large explosion occurred in the Port of Beirut, Lebanon, causing considerable damage to the city, and resulting in over 200 casualties and more than 7,500 injuries. The event received widespread media coverage, partly due to the unprecedented (in modern times) devastation caused by the blast, and partly due to how well-documented the explosion was. Many videos were posted to social media following the explosion, a large number of which clearly showed the moment of detonation, expansion of the fireball, and subsequent propagation of the shock wave through the city. Figure 8 shows a series of stills taken from one of these videos [28].

---

[4]The assumption here is that in the extreme near-field, the surrounding layer of compressed air remains attached to the detonation product fireball, and therefore measurement of the velocity of this interface equates to measurement of incident Mach number.
[5]In Ref. [25] the gradient of radius-time relationship was determined through central differencing, which was plotted as a velocity-radius curve. A least-squares polynomial relationship was fitted, which was then used to determine the incident Mach number at a series of hypotenuse distances from the charge centre to points on the hypothetical reflecting surface.

Figure 8   Example video footage of the 2020 Beirut explosion [28]. Images timestamped by the author

The author and colleagues were able to identify 16 publicly-available videos which met the following criteria [29]:

- Filming began prior to detonation, with a direct line-of-sight from the filming location to the source of the explosion[6], such that the moment of detonation could be identified[7];
- Filming continued until after arrival of the blast wave;
- The video was taken from an identifiable location, which was determined by the authors by cross-referencing recognisable features in the videos with Google Street View and satellite images from Google Earth;
- Audio and video in sync.

Once the precise time of detonation was identified, a number of techniques were used to determine blast wave TOA at 38 locations:

- The arrival of the blast wave could be identified as a sharp increase in amplitude of the audio signal. For some videos with higher levels of background noise this required a frame-by-frame examination to eliminate other spikes in the audio signal;
- The blast wave could be seen to arrive at an identifiable location in the field-of-view through visual inspection (failure of glazing on a building, observable damage to cars, etc.);
- The size of the detonation product fireball could be estimated for the first few frames after detonation in a small number of videos, using the nearby grain silo to calibrate the scale of the images.

The distance from each location to the point of detonation (assumed to be the centre of the warehouse) was calculated using the "measure distance" feature in Google Earth, and ranged from 80-2,380 m from the centre of the explosion.

A regression analysis was performed [29], which aimed at minimising the mean absolute residual error between the observed and predicted TOAs. Here, the authors fit a simplified polylogarithmic function to the ConWep scaled TOA vs. scaled distance relationship, which was extrapolated beyond the original ConWep dataset by assuming that, at larger scaled distances, the blast travelled at ambient sound speed (350.7 m/s according to atmospheric conditions at the time of the blast [29]). Predicted TOAs were generated at each location for a large range of equivalent (hemispherical) TNT charge masses, and it was found that an explosive yield of 500 t TNT had the minimum mean absolute residual error.

The observed and predicted TOAs are shown in Figure 9(a), with associated residuals shown in Figure 9(b). At the median distance, 1000 m, the maximum residual of ±0.2 s corresponds to a relative difference in TOA of approximately ±10%. This is roughly five times larger than variations observed in the arena tests described earlier in this article, however this is deemed reasonable given the complexity of a large-scale explosion in an urban setting and the relative coarseness of the data (videos at ~30 fps, and distances able to be determined to within a few metres).

This analysis demonstrates that it is possible to estimate the yield of large-scale explosions to a reasonable degree of confidence, using publicly-available data and simple regression techniques. Future rapid assessments such as this may assist in implementing emergency response plans by facilitating better estimates of the likely injuries and structural damage at various distances from the explosion, and identifying areas of highest risk. Furthermore, the ability to rapidly determine the scale and severity of an urban explosion will provide crucial factual context for political and media discussion.

---

[6]In a small number of videos the detonation itself was obscured by neighbouring buildings but could be identified as a clear flash in the images.
[7]One of the videos began slightly after detonation, and the time of detonation was estimated by examining the size of the fireball in the first few frames and back-extrapolating.
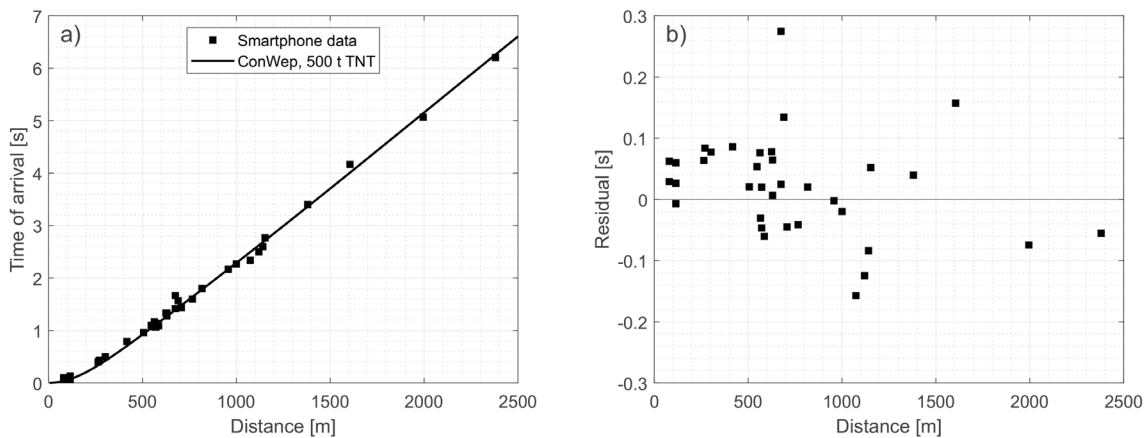
Figure 9   a) Blast wave time of arrival from analysis of smartphone video footage uploaded to social media after the 2020 Beirut explosion [29], compared to ConWep predictions for 500 t TNT hemisphere; b) Residual: difference between observed and predicted data shown in (a)

Summary and outlook

Despite often being overlooked in favour of other metrics such as peak pressure, duration, and impulse, blast wave TOA is an important metric which can offer valuable insights into the behaviour and properties of a blast wave as it propagates. This article has summarised three main TOA studies conducted by the author and colleagues.

In the first, a large number of arena tests were compiled and used to demonstrate the high relative repeatability of TOA measurements. In the second, high speed video was used in conjunction with image processing techniques to identify the edge of the expanding fireball and therefore quantify TOA in the near-field. Rankine-Hugoniot theory was used to transform the TOA measurements into inferred reflected pressure distributions, which were shown to be in good agreement with directly-measured values from similar tests using different diagnostics. Finally, recent work on estimating the yield of the 2020 Beirut explosion was summarised. 38 TOA datapoints were extracted from publicly-available videos posted to social media, from which the authors were able to estimate that the explosion yield was equivalent to 500 t TNT.

It can be concluded that TOA is a reliable and powerful metric for quantifying blast wave behaviour in both laboratory and real-world settings.

Acknowledgements

References

[1]   E Esparza. Blast measurements and equivalency for spherical charges at small scaled distances. International Journal of Impact Engineering, 4(1):23-40, 1986.

[2]   CN Kingery and G Bulmash. Airblast parameters from TNT spherical air burst and hemispherical surface burst. Technical Report ARBRL-TR-02555, U.S Army BRL, Aberdeen Proving Ground, MD, USA, 1984.

[3]   DW Hyde. Conventional Weapons Effects Program (ConWep). U.S Army Waterways Experimental Station, Vicksburg, MS, USA, 1991.

[4]   GF Kinney and KJ Graham. Explosive Shocks in Air. Springer, NY, USA, 1985.

[5]   JM Dewey and AG Gaydon. The air velocity in blast waves from T.N.T. explosions. Proceedings of the Royal Society of London. Series A. Mathematical and Physical Sciences, 279(1378):366-385, 1964.

[6]   JM Dewey. The properties of a blast wave obtained from an analysis of the particle trajectories. Proceedings of the Royal Society of London. Series A. Mathematical and Physical Sciences, 324(1558):275-299, 1971.

[7]   MJ Hargather and GS Settles. Optical measurement and scaling of blasts from gram-range explosive charges. Shock Waves, 17(4):215-223, 2007.

[8]   MJ Hargather. Background-oriented schlieren diagnostics for large-scale explosive testing. Shock Waves, 23(5):529-536, 2013.

[9]   MM Biss and KL McNesby. Optically measured explosive impulse. Experiments in Fluids, 55(6):1749-1-8, 2014.

[10]   KL McNesby, MM Biss, RA Benjamin, and RA Thompson. Optical measurement of peak air shock pressures following explosions. Propellants, Explosives, Pyrotechnics, 39(1):59-64, 2014.

[11]   KL McNesby, BE Homan, RA Benjamin, VM Boyle, JM Densmore, and MM Biss. Quantitative imaging of explosions with high-speed cameras. Review of Scientific Instruments, 87(5):051301-1-14, 2016.

[12]   SE Rigby, A Tyas, SD Fay, SD Clarke, and JA Warren. Validation of semi-empirical blast pressure predictions for far   field

explosions – Is there inherent variability in blast wave parameters? In: 6th International Conference on Protection of Structures Against Hazards (PSH14), Tianjin, China, 2014.

[13] SE Rigby, A Tyas, T Bennett, SD Clarke, and SD Fay. The negative phase of the blast load. International Journal of Protective Structures, 5(1):1-20, 2014.

[14] SE Rigby, SD Fay, A Tyas, JA Warren, and SD Clarke. Angle of incidence effects on far-field positive and negative phase blast parameters. International Journal of Protective Structures, 6(1):23-42, 2015.

[15] A Tyas, J Warren, T Bennett, and S Fay. Prediction of clearing effects in far-field blast loading of finite targets. Shock Waves, 21(2):111-119, 2011.

[16] A Tyas. Blast loading from high explosive detonation: What we know and what we don't know. In: 13th International Conference on Shock and Impact Loads on Structures, Guangzhou, China, 2019.

[17] B Hopkinson. British Ordnance Board Minutes, 13565. 1915.

[18] C Cranz. Lehrbuch der Basllistik. Springer, Berlin, Germany, 1926.

[19] SE Rigby and P Sielicki. An investigation of TNT equivalence of hemispherical PE4 charges. Engineering Transactions, 62(4):423-435, 2014.

[20] D Bogosian, M Yokota, and S Rigby. TNT equivalence of C-4 and PE4: A review of traditional sources and recent data. In: 24th International Symposium on Military Aspects of Blast and Shock (MABS24), Halifax, Nova Scotia, Canada, 2016.

[21] SD Clarke, SD Fay, JAWarren, A Tyas, SE Rigby, and I Elgy. A large scale experimental approach to the measurement of spatially and temporally localised loading from the detonation of shallow-buried explosives. Measurement Science and Technology, 26:015001, 2015.

[22] SE Rigby, SD Fay, SD Clarke, A Tyas, JJ Reay, JA Warren, M Gant, and I Elgy. Measuring spatial pressure distribution from explosives buried in dry Leighton Buzzard sand. International Journal of Impact Engineering, 96:89-104, 2016.

[23] SE Rigby, A Tyas, SD Clarke, SD Fay, JJ Reay, JA Warren, M Gant, and I Elgy. Observations from preliminary experiments on spatial and temporal pressure measurements from near-field free air explosions. International Journal of Protective Structures, 6(2):175-190, 2015.

[24] A Tyas, JJ Reay, SD Fay, SD Clarke, SE Rigby, JA Warren, and DJ Pope. Experimental studies of the effect of rapid afterburn on shock development of near-field explosions. International Journal of Protective Structures, 7(3):456-465, 2016.

[25] SE Rigby, R Knighton, SD Clarke, and A Tyas. Reflected near-field blast pressure measurements using high speed video. Experimental Mechanics, 60(7):875-888, 2020.

[26] J Canny. A computational approach to edge detection. IEEE Transactions on Pattern Analysis and Machine Intelligence, 8(6):679-698, 1986.

[27] SE Rigby, A Tyas, RJ Curry, and GS Langdon. Experimental measurement of specific impulse distribution and transient deformation of plates subjected to near-field explosive blasts. Experimental Mechanics, 59(2):163-178, 2019.

[28] https://twitter.com/borzou/status/1290675854767513600. 4 August 2020, retrieved 17 December 2020.

[29] SE Rigby, TJ Lodge, S Alotaibi, AD Barr, SD Clarke, GS Langdon, and A Tyas. Preliminary yield estimation of the 2020 Beirut explosion using video footage from social media. Shock Waves, 30(6):671-675, 2020.